High temperature dependence of thermal transport in graphene foam

2015 Nanotechnology 26 105703

(http://iopscience.iop.org/0957-4484/26/10/105703)

IOP Publishing Nanotechnology
Nanotechnology 26 (2015) 105703 (9pp) doi:10.1088/0957-4484/26/10/105703

High temperature dependence of thermal transport in graphene foam

Man Li, Yi Sun, Huying Xiao, Xuejiao Hu and Yanan Yue

School of Power and Mechanical Engineering, Wuhan University, Wuhan, Hubei, 430072, People's Republic of China

E-mail: yyue@whu.edu.cn

Received 9 October 2014, revised 12 January 2015
Accepted for publication 19 January 2015
Published 16 February 2015

Abstract

In contrast to the decreased thermal property of carbon materials with temperature according to the Umklapp phonon scattering theory, highly porous free-standing graphene foam (GF) exhibits an abnormal characteristic that its thermal property increases with temperature above room temperature. In this work, the temperature dependence of thermal properties of free-standing GF is investigated by using the transient electro-thermal technique. Significant increase for thermal conductivity and thermal diffusivity from ~0.3 to 1.5 $W\,m^{-1}\,K^{-1}$ and $\sim 4\times10^{-5}$ to $\sim 2\times10^{-4}\ m^2\,s^{-1}$ respectively is observed with temperature from 310 K to 440 K for three GF samples. The quantitative analysis based on a physical model for porous media of Schuetz confirms that the thermal conductance across graphene contacts rather than the heat conductance inside graphene dominates thermal transport of our GFs. The thermal expansion effect at an elevated temperature makes the highly porous structure much tighter is responsible for the reduction in thermal contact resistance. Besides, the radiation heat exchange inside the pores of GFs improves the thermal transport at high temperatures. Since free-standing GF has great potential for being used as supercapacitor and battery electrode where the working temperature is always above room temperature, this finding is beneficial for thermal design of GF-based energy applications.

Keywords: graphene foam, thermal transport, temperature

(Some figures may appear in colour only in the online journal)

1. Introduction

Graphene is a two dimensional sheet of sp^2 bonded carbon atoms arranged in honeycomb lattice. It intensely intrigues scientists and engineers since its discovery due to its excellent physical properties and great potential in industrial applications [1]. The extreme thin thickness of graphene makes its operation and characterization difficult, thus it need to be supported by a substrate in many situations. Among various efforts to the implementation of graphene material, the free-standing graphene foam (GF) emerges and is successful to integrate the two-dimensional graphene sheets into macroscopic structures meanwhile preserving most of the excellent physical/chemical properties of graphene [2]. Benefited from the freestanding and flexible structure and high electrical conductivity, GF has been proven great potential in supercapacitor [3–6], electromagnetic interference shielding [7] and battery electrodes [6, 8, 9]. Thermal property of GF is of great importance for the design of GF-based devices to effectively manage the heat dissipation involved in the electrochemical reactions or Joule heating.

Compared with the extensive research about thermal transport in graphene [10–14], less attention has been focused on GF. The first experimental study of thermal transport in GF was conducted by Pettes *et al* [15] by using steady-state electrical heating method. They measured the thermal conductivity of GF under different synthesis conditions and extracted the intrinsic thermal conductivity of the few-layer graphene (FLG) and ultrathin graphite (UG) constituents. Lin *et al* adopted the transient electro-thermal (TET) technique to characterize the thermal diffusivity of GF [16]. They attributed the significantly reduced thermal conductivity of graphene to the phonon scattering at the interfaces, rough edge and contaminants on the surface [16]. In GF, the interfacial

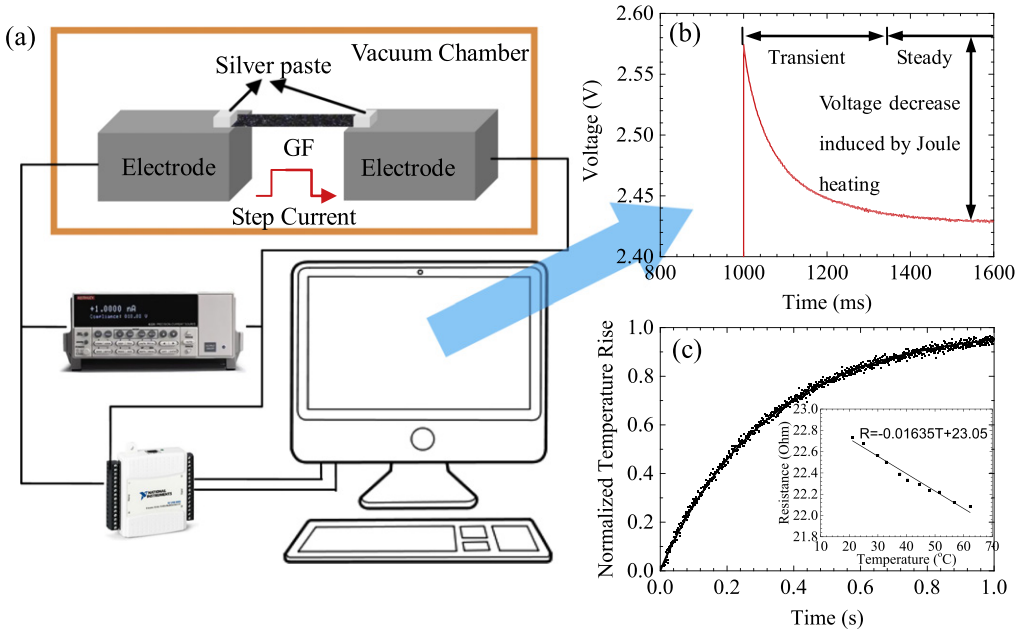

Figure 1. (a) Schematic of the TET technique and experimental setup. (b) An example of voltage curve shows the voltage rises when a step current is supplied and then decreases gradually. The transient period can be used to derive thermal diffusivity and the voltage drop from the highest value to steady-state value can be used to calculate thermal conductivity. (c) The normalized temperature rise of samples derived from the voltage change can be used to fit the thermal diffusivity. The inset figure is the linear relationship (slope: 0.016 35 Ω K^{-1}) between the electrical resistance of GF and temperature. The normalized temperature coefficient can be obtained as $7.23 \pm 0.88 \times 10^{-4}$ K^{-1}.

thermal resistance (ITR) of graphene flakes, whose value is in the range of 10^{-5}–10^{-9} K m^2 W^{-1} depending on interface conditions is important [17, 18]. Usually, the contact resistance can be much larger than the thermal resistance of graphene ($\sim 1 \times 10^{-8}$ K m^2 W^{-1} if assuming thermal conductivity as 1000 W m^{-1} K^{-1}, and length as 10 μm for an approximate calculation) [10, 15]. Another study [19] focuses on thermal interface properties of GF by presuming thermal conductivity of the GF of 1 g cm^{-3} as high as 175 W m^{-1} K^{-1}.

For most GF-based applications, the working temperature is above room temperature, e.g. from room temperature to 200 °C as anode materials in Li-ion batteries. Thereby, the thermal performance of GF within such temperature range is precedent before the implementation of GFs. For single-crystal structure of carbon materials such as carbon nanotubes (CNTs) and graphene etc, the temperature dependence of thermal property can be explained from the intensified inharmonic process [14, 20]. But the thermal contact resistance of inner structures which plays an important role in thermal transport of bulk materials is much more complicated and is hard to be determined, especially under some heating experiments where the sample morphology or physical contacts may change. For example, the thermal conductivity of CNTs sheet and fiber increase with temperature from 100 K to 500 K as measured by Yue *et al* and Aliev *et al* [21, 22]. As the bulk material of graphene, GF consists of countless flakes which overlap or interconnect with each other under van der Waals interactions. Therefore, how the ITR between graphene flakes determines the thermal transport of GFs is of great interest to explore.

2. Experiment principle and details

2.1. Physical model

The TET technique developed in Wang's lab is an effective approach to simultaneously measure thermal conductivity and thermal diffusivity of one-dimensional materials [23]. The physical model is based on one-dimensional heat conduction equation with uniform heat source. In this technique, a wire is suspended between two electrodes and heated by a step current. The electrode has large heat capacity and high thermal conductivity for heat dissipation. The sample experiences a quick temperature rise before reaching thermal equilibrium with the environment. This process can be simultaneously monitored from the voltage because resistance of the wire is temperature dependent. The partial differential equation for this thermal model is $\partial(\rho c_p T)/\partial t = k\partial^2 T/\partial x^2 + q_0$, where ρ, c_p, k are the density, specific heat and thermal conductivity of the wire, respectively. Here, q_0 is the heat generation per unit volume. The temperature rise of the wire can be obtained by solving this partial differential equation as $T(t)$

$$= T_0 + 8q_0L^2/k\pi^4 \sum_{m=1}^{\infty}\left\{1 - \exp\left[-(2m-1)^2\pi^2\alpha t/L^2\right]\right\}/(2m-1)^4,$$

where α is the thermal diffusivity $\left(\alpha = k/\rho c_p\right)$ of the wire. After normalizing the temperature increase as $T^* = \left(T(t) - T_0\right)/\left(T(t \to \infty) - T_0\right)$, thermal diffusivity of the wire can be fitted from $T^* = 96/\pi^4 \sum_{m=1}^{\infty}\left\{1 - \exp\left[-(2m-1)^2\pi^2\alpha t/L^2\right]\right\}$

$/(2m-1)^4$. Thermal conductivity can be derived as $k = q_0 L^2/12\Delta T$ when the temperature is stable.

2.2. Experimental setup and details

Figure 1(a) illustrates the experiment setup of TET technique. The strip-like GF is suspended between two electrodes (aluminum blocks) which have large volume, high electrical conductivity and thermal conductivity to dissipate heat and make samples stay at the room temperature. Three samples were cut from the same GF piece with different sizes of $10.5 \times 1.35 \times 1.4\ \text{mm}^3$ (sample 1), $6.1 \times 1.26 \times 0.66\ \text{mm}^3$ (sample 2) and $4.5 \times 1.18 \times 0.74\ \text{mm}^3$ (sample 3), ensuring that one-dimensional thermal transport model is applicable. Two ends of the GF were attached on the electrodes with high conductive silver paste to minimize the electrical/thermal contact resistance. The sample stage is placed in a vacuum chamber where the atmosphere pressure is reduced to below 10^{-3} Torr to eliminate convective heat loss. The step current is supplied by a current source (KEITHLEY 6220) and the analog signals of the voltage of the GF is recorded at a time interval of 0.1 μs with a data acquisition card (NI USB-6009). An example of the curve is demonstrated in figure 1(b). There is instant voltage signal as the step current is supplied, and it gradually decreased upon reaching steady-state. Carbon based conductive materials usually has a negative temperature constant with resistance, for example, the CNT bundle/fibers [16, 21]. Otherwise, it would show a gradually increase curve rather than this decrease curve. The transient process is closely related to the thermal diffusivity of the material as analyzed in the physical model. To minimize random noise of the voltage signal, each data is averaged by surrounding ten points in the time interval of 1 μs. Furthermore, to reduce measurement uncertainty, each curve is repeated and averaged 12 times. Noticing the linear relationship between temperature and resistance of GF, the normalized temperature rise can be directly derived as $T^* = \big(U(t) - U_0\big)/\big(U(t \to \infty) - U_0\big)$ as shown in figure 1(c). The inset figure in figure 1(c) shows the linear fitting of electrical resistance with temperature ranges from 20 to 65 °C with a slope of $-0.016\,35\ \Omega\,\text{K}^{-1}$. This slope can be used for temperature calibration of all samples since they are from the same bulk material. Each sample has different resistance as the cutting dimensions are different. In order to make this calibration result applicable, the temperature coefficient of the electrical resistance is normalized as $p = -7.23 \pm 0.88 \times 10^{-4}\ \text{K}^{-1}$ with confidence interval of 95%.

The GF sample used in this work was purchased from Advanced Chemicals Suppliers Material Company. Using chemical vapor deposition method, the graphene was deposited on a porous nickel scaffold with the pore size varying from 20 to 500 μm, which was removed afterwards by chemical etching. More relevant details can be referenced in literatures[2, 15]. Figure 2 shows the scanning electron microscopy (SEM) images of our GF samples. Despite the pore size of hundreds micrometers we observed, the SEM images illustrate the existence of smaller pores of tens micrometers. The SEM images show that our GF consists of large amounts of graphene flakes (size: around 10 μm). There are corrugating and overlapping with each other for graphene flakes.

3. Results and discussions

3.1. Thermal characterization result of GF

Figure 3 gives an example of characterization curve of Sample 1. A small step current of 10 mA is applied and the voltage is recorded as shown in figure 3(a). The electrical resistance difference of GF between initio moment and steady state is $\Delta R = \Delta U/I = 0.7193\ \Omega$, indicating the average temperature rise of GF is $\Delta T = \Delta R/(R_0 \cdot p) = 11.85^{+1.64}_{-1.29}$ K. According to the measurement principle as described above, the thermal conductivity (k) of GF at 312 K can be obtained as $0.3255^{+0.0451}_{-0.0353}\ \text{W m}^{-1}\ \text{K}^{-1}$. The uncertainty of k is from the uncertainty in temperature coefficient calculation. Our measured low value is close to measurement result of Pettes *et al* as $0.26\ \text{W m}^{-1}\ \text{K}^{-1}$ at room temperature [15]. The morphology of our sample shows obvious discrete distribution of flakes, meaning that the thermal contact resistance is significant. The high porosity of the material as shown in figure 2 combined with large thermal contacts inside the foam could be the main reason for the reduced thermal conductivity. Thermal diffusivity of Sample 1 is determined as $3.34^{+0.01}_{-0.01} \times 10^{-5}\ \text{m}^2\ \text{s}^{-1}$, where the uncertainty is from the data fitting based on a confidence interval of 95%. Our result is also closed to the value measured by Wang's group ($3.86 \times 10^{-5}\ \text{m}^2\ \text{s}^{-1}$) [16], the slight difference can be caused by the difference in sample porosity and experimental conditions.

3.2. Temperature dependence of thermal property of GF

Temperature dependence of thermal properties of GF from 300 K to 450 K was studied. The thermal conductivity with respect to the temperature is shown in figure 4. Figure 4(a) illustrates that thermal conductivity of three GF samples increases from $\sim 0.3\ \text{W m}^{-1}\ \text{K}^{-1}$ at around room temperature to $1.5\ \text{W m}^{-1}\ \text{K}^{-1}$ at the highest temperature about 450 K. The measured low thermal conductivities of freestanding GF in this work is attributed to two main reasons: first, the bulk volume of GF consists of huge number of thermal contacts of graphene flakes as validated from the SEM images as shown in figures 2(a)–(d). These thermal contacts act as the narrow bridges for thermal energy transport. In other words, the large thermal conductance inside graphene has minor influence on the thermal transport of bulk material compared with the large thermal contact resistance. Second, high porosity of GF limits the efficiency of energy transmission inside the sample in terms of reducing cross-section area of thermal transport. In the experiment, the high vacuum condition (around 10^{-3} Torr) further reduced the air molecules in the small pores, which let only phonon transport through graphene contacts and photon energy exchange between one side of semicircle of the pore and the other side applicable. For our experiment with

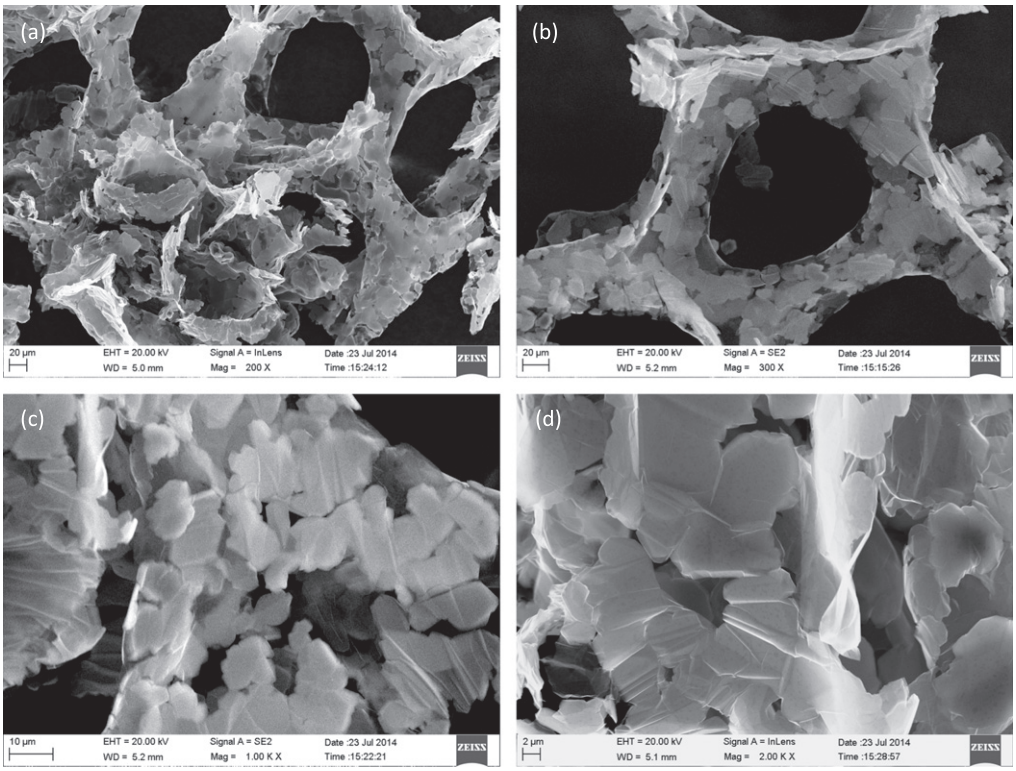

Figure 2. SEM images of the GF studied in our experiments. (a), (b) show the microscopic structure; (c), (d) show the morphology of graphene and ultra-thin graphite constituents.

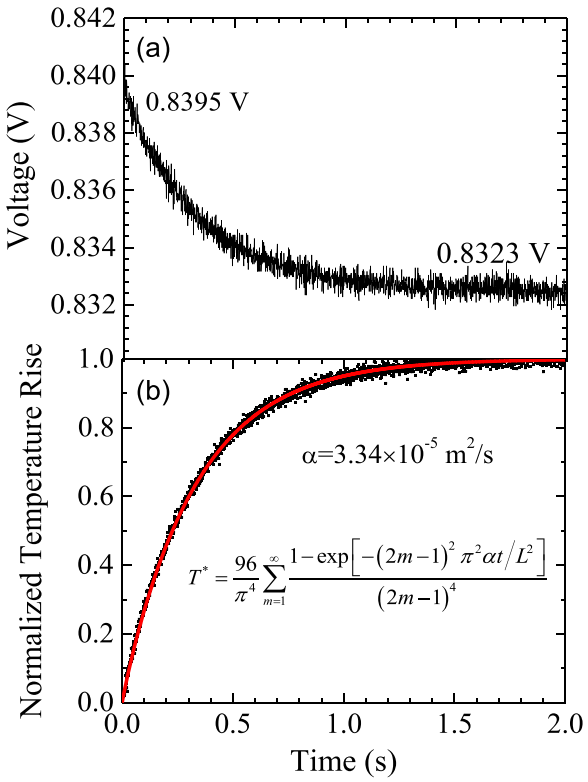

Figure 3. The characterization curve of thermal conductivity and thermal diffusivity of sample 1: (a) the voltage curve to determine thermal conductivity and (b) the normalized temperature rise curve for fitting thermal diffusivity of GF.

temperature increase no higher than 450 K, radiation effect is not that significant to exceed the energy transport through heat conduction. Hereby, the thermal conductivity measured in our experiment is a macroscopic (or say apparent) value of the whole GF sample rather than describing the thermal conductance of its inner structures. Noting that there is rare scenario that GF will be used in high vacuum conditions, for example, it can be in contact with electrolyte if being used in Li-ion batteries, the thermal performance of GF would be improved in these applications.

It is noticed that there is an increasing trend of thermal conductivity with temperature for all three samples with temperature increase from 310 K to 440 K. Their percentage improvements of thermal conductivity are similar (as shown in figure 4(b)). The thermal conductivity at the highest temperature is almost five times that at room temperature. Thermal conductivity of carbon-based materials, such as diamond, graphene, graphite [14, 24] and single-wall CNT [20] have a well-described behavior related to temperature (within a large temperature range): firstly increase and then drop in a $1/T$ relation due to the Umklapp phonon–phonon scattering [13, 20]. The transition temperature is often below 300 K [14, 25]. But for GF which can be regarded as the composite with high porosity rather than a good crystalline material, this abnormal temperature dependence of thermal property cannot be solely explained with Umklapp scattering theory. Again, the intrinsic thermal contacts and small amount of radiation effect could be the reason for this discrepancy of this

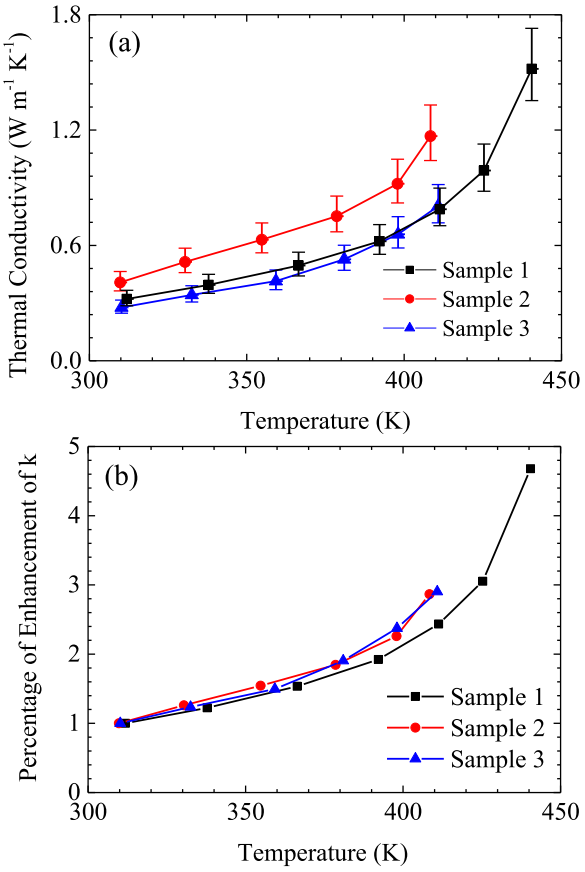

Figure 4. (a) Temperature dependence of thermal conductivity of three GF samples. Thermal conductivity increases significantly for all samples. (b) The improvement percentage shows that thermal conductivity improvement is similar for three samples.

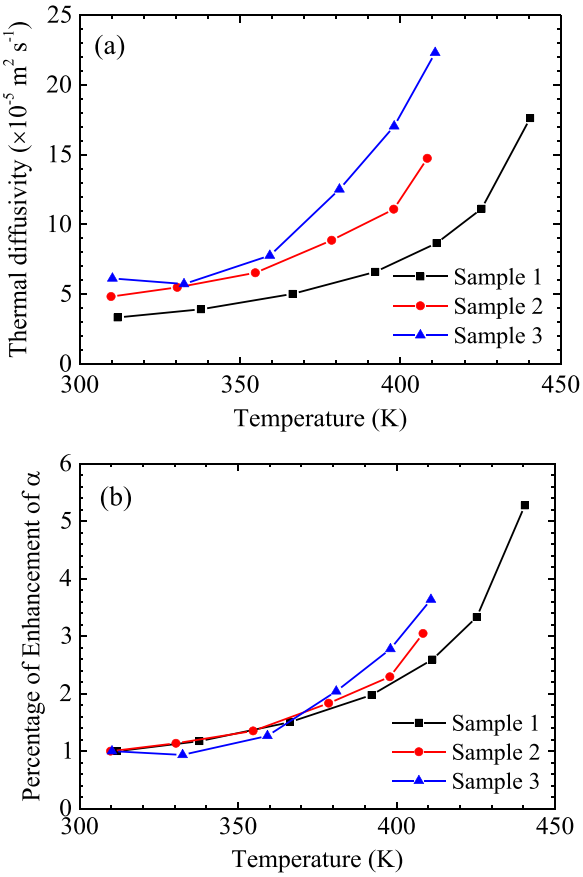

Figure 5. (a) Temperature dependence of thermal diffusivity of three samples. Thermal diffusivity improves significantly with temperature. (b) The improvement percentage shows a similar trend for all samples.

temperature dependence effect. Besides, this phenomenon has been discovered in other carbon-based materials, such as CNT buckypapers, CNT sheets and CNT fibers [21, 22, 26]. Especially in CNT sheets, the improvement of thermal conductivity from 100 K to 300 K can be as high as several tens' times for long CNT sheets. The common feature of long-length CNT aggregates and GF is the countless interconnect points, which produce large ITR in the thermal transport of GF.

Pettes *et al* have conducted the study for the temperature dependence of similar GF. They found that the temperature dependence followed the $1/T$ relation and they argued that the thermal transport of GF could be explained by the Umklapp phonon scattering theory. The discrepancy of our measurement result can be explained by the difference in sample structures. SEM images show that the surface of their samples is much smoother and the size of their graphene flakes much larger. Thus, it is the in-plane thermal resistance of graphene and UG constituents dominates thermal transport in their samples rather than the ITR between graphene flakes for our samples. That is why they found that the temperature dependence of their samples was the same with that of pure graphene. Therefore, the difference in sample structure (even with the same constituents) might lead to different thermal transport mechanism, and cannot be explained by a sole theory.

Thermal diffusivities of these samples are obtained as shown in figure 5(a). The value ranges from $\sim 4 \times 10^{-5}$ to $\sim 2 \times 10^{-4}$ m^2 s^{-1} at the same temperature range, which are relatively larger values compared with other semiconductive materials such as silicon. Considering the measured low thermal conductivity, it proves that there is high porosity inside GF ($\alpha = k/\rho c$). It is also observed that there is a little difference for thermal diffusivity of different samples. It might come from the structural modification during the sample preparation while cutting from the same batch. In addition, as analyzed by Lin *et al* the sample lengths could impact the radiation loss, thus introduce some errors to the final result [16]. Since the temperature dependence of thermal properties is our interest, the difference between each sample due to radiation heat loss is ignored here. Detailed analysis about the radiation induced uncertainty will be provided in the following section. As observed in figure 5(b), similar as thermal conductivity, there is an increasing trend for thermal diffusivity with respect to the temperature, and the highest value is almost five times the lowest, which is an important evidence for this significant temperature dependence of thermal property of GF.

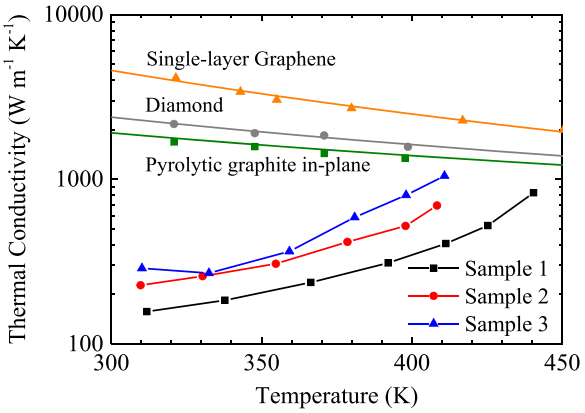

Figure 6. The intrinsic thermal conductivity of solid phase in GF with respect to temperature for three samples. The experimental data of thermal conductivity of single-layer graphene, diamond and pyrolytic graphite (in-plane) from [7] and [2] is listed as a comparison, and is fitted as $k = 8.14 \times 10^8\ T^{-2.12}$, $k = 4.86 \times 10^6\ T^{-1.34}$ and $k = 1.08 \times 10^6\ T^{-1.11}$ for the temperature relationship.

3.3. Physical interpretation of experimental observations

To understand the mechanism underlying this phenomenon, the intrinsic thermal conductivity of the solid phase is analyzed. The model for heat conduction in porous solid media presented by Schuetz *et al* [27] shows that the intrinsic thermal conductivity can be computed as $k_{\text{solid}} = 3\ k_{\text{GF}}$ where k_{GF} is the thermal conductivity of GF, φ the volume fraction of the solid phase in the foam. According to the definition of thermal diffusivity of $\alpha_{\text{GF}} = k_{\text{GF}}/\rho_{\text{GF}} c_{\text{GF}}$, the mass density of our samples (ρ_{GF}) can be estimated as $10.5^{+1.6}_{-1.6}$ kg m^{-3} by assuming the specific heat per mass of GF equivalent to that of graphite as 709 J kg^{-1} K^{-1} [28]. Noting the mass density of the solid phase (ρ_{solid}) equivalent to that of graphite [28], the volume fraction of GF is calculated from $\phi = \rho_{\text{GF}}/\rho_{\text{solid}}$ as $0.48^{+0.07}_{-0.07}$ %. Inspired from 16 that $\alpha_{\text{solid}} = k_{\text{solid}}/\rho_{\text{solid}} c_{\text{solid}}$, $\alpha_{\text{GF}} = k_{\text{GF}}/\rho_{\text{GF}} c_{\text{GF}}$ and $\rho_{\text{solid}} c_{\text{solid}} = \rho_{\text{GF}} c_{\text{GF}}/\phi$, we can readily get the intrinsic thermal conductivity of the solid phase as $k_{\text{solid}} = 3\alpha_{\text{GF}}/\rho_{\text{solid}} c_{\text{solid}}$. Substituting the mass density of 2210 kg m^{-3} and specific heat of graphite as 709 J kg^{-1} K^{-1}, intrinsic thermal conductivity of solid phase of GF is obtained as from 200 to 800 W m^{-1} K^{-1} as shown in figure 6. The results obviously is much lower than the high thermal conductivity of individual graphene [29, 30] and diamond [25] while close to that of graphite [14, 25]. Therefore, the more frequent phonon–phonon and phonon-boundary scattering, which are attributed to the defects, rough edges, surface contamination and complex morphology should dominate thermal transport in the solid phase of GF. In other words, the ITR across graphene flakes is responsible for the reduced thermal property of GF. It could be the main reason for this significant temperature-dependence trend and the larger thermal conductivity at higher temperature is as a result of reduced thermal contact resistance. Considering the main constituents of GF are FLG and UG, it should exhibit thermal expansion like graphite [31] other than thermal contraction that single-layer graphene does [32, 33]. Assuming the thickness of constituent graphene is in the order of 1 nm (set as 1 nm as an example), and the TEC along out-of-plane direction is found as 3×10^{-5} K^{-1} at our temperature range [34], the thickness of one graphene flake had an expansion of 3×10^{-3} nm with temperature rise of 100 K, which is 3% in thickness improvement. This would greatly improve the contact strength between two graphene flakes. As both of the overlapped graphene flakes had expansion, the interfacial distance between them should be reduced from 0.335 nm (distance at equilibrium under van der Waals interaction) [8] to 0.329 nm. Therefore, as the temperature goes higher, the thermal expansion effect become stronger, squeezing the graphene flakes together with larger pressure.

Similar phenomenon has been observed in CNTs packed bed with reduced thermal conductivity. It is found that k of CNTs packed bed is around 0.1–0.2 W m^{-1} K^{-1} [35]. The ITR between CNTs is considered as the main reason. From the SEM images, we can estimate the size of graphene flakes as around 10 μm. Assuming the thermal conductivity of graphene flakes is 1000 W m^{-1} K^{-1} [14], the thermal resistance of a single graphene flake is approximated as ~1 $\times 10^{-8}$ K m^2 W^{-1}. This value is at the same order of the ITR of tightly bonded interface [18]. The thermal resistance of solid phase in GF is composed of the thermal resistance of graphene flakes and their ITR, which can be expressed as: $R_{\text{solid}} = R_G + R_C$, where the terms represent the thermal resistance of the solid phase, graphene flakes and contacts respectively. Since thermal conductivity of inner graphene flakes can hardly be determined, we estimate it as between that of single-layer graphene (highest value) and graphite (lowest value). Thermal conductivities of single-layer graphene [30] and pyrolytic graphite [25], as shown in figure 6, are adopted to calculate the corresponding thermal resistance of a single graphene flake with the size of 10 μm. The thermal contact resistance can also be calculated accordingly. figure 7 lists the temperature dependence of thermal resistance of solid phase, thermal contact resistance and thermal resistance of graphene. It shows that the thermal resistance of graphene is much less than thermal contact resistance for temperature below 400 K. When temperature rises above 400 K, the effect of thermal resistance from interfacial contact and graphene flakes are close. Thermal contact resistance significantly decreases from 6×10^{-8} to 4×10^{-9} K m^2 W^{-1} while the thermal resistance of graphene increases slightly. Therefore, the temperature dependence of thermal resistance of the solid phase is determined mostly by the thermal contact resistance between graphene flakes [17]. The significant reduction in thermal contact resistance can be only explained by the tighter binding interface due to thermal expansion.

As temperature increases, the radiation heat exchange within the pore inside GF should be considered. The energy exchange through radiation can be computed according to the Stefan-Boltzmann law, $E_r = \varepsilon_r \sigma (T^4 - T_0^4) \approx 4\varepsilon_r \sigma T_0^3 (T - T_0)$, where E_r is the heat radiation power per area of material, ε_r the emissivity of material, σ the Stefan-Boltzmann constant, T_0 the room temperature. The effective thermal conductivity due to radiation

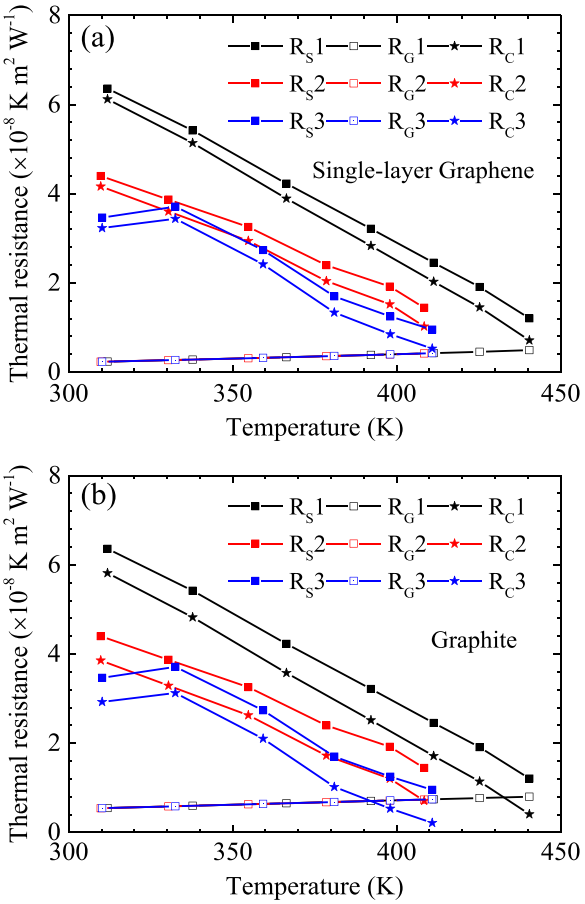

Figure 7. The summary of thermal resistance of solid phase (filled square), graphene (open square), and contact resistance between graphene flakes (star) of all samples. The thermal contact resistance is calculated by assuming the thermal conductivity of the graphene flakes is the same as (a) the single-layer graphene (largest value in literature) and (b) the pyrolytic graphite. It is obvious that thermal contact resistance dominates the thermal transport of GF and is responsible for temperature dependence trend obtained in our experiment.

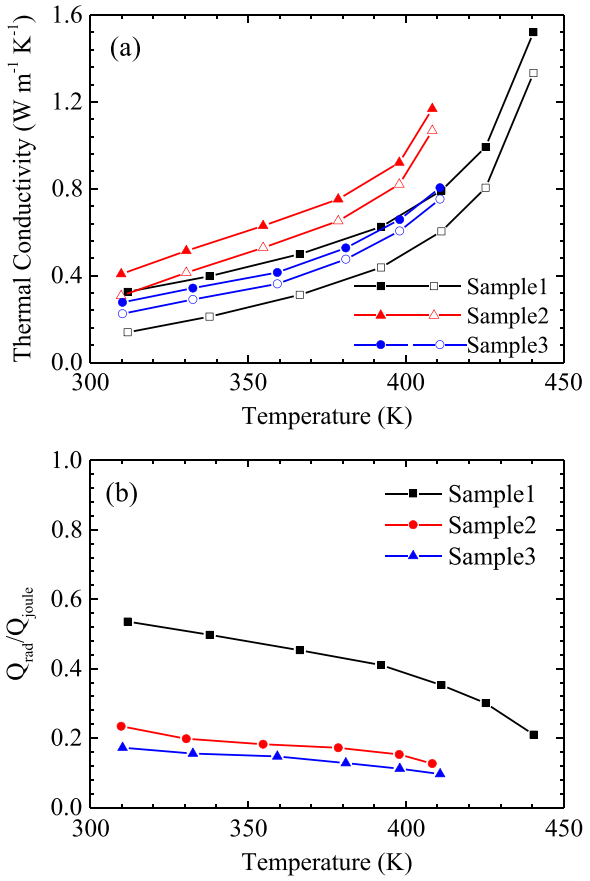

Figure 8. (a) The comparison of thermal conductivity computed through heat conduction model with (filled geometry) and without (open geometry) heat radiation. (b) The ratio of radiation heat loss to the surroundings to the total power of Joule heating.

can be expressed as $4\varepsilon_r\sigma A_s T_0^3$ when temperature rise is not high, where A_s is the pore surface. It is obvious that the third order of temperature can greatly improve the effective (or say apparent) thermal conductivity at high temperature. This radiation heat exchange could be another reason for the improved thermal conductivity at high temperatures.

3.4. Error analysis of experimental results

The measurement result could be somewhat overestimated due to the radiation heat loss from the sample surface to the surroundings. The governing equation can be modified as [15]: $kA\mathrm{d}^2T/\mathrm{d}x^2 - 4\varepsilon_r\sigma T_0^3 P\left(T - T_0\right)/A + q_0 = 0$, where A and P is the area and perimeter of the cross-section. The solution is $k = -q_0[2\tanh(mL/2)/mL - 1]/m^2\Delta T$, and $m^2 = 4\varepsilon_r\sigma T_0^3 P/kA$. The effective emissivity of GF is chosen as 0.97 according to the previous research conducted by Pettes *et al* [15]. Figure 8(a) compares the thermal conductivity calculated from the heat conduction model with (filled geometry) and without (open geometry) heat radiation. The values after corrections are only slightly smaller than the original values. Figure 8(b) shows the ratio of radiation heat loss to the surroundings to the total Joule heating power, which indicates that only in sample 1 has obvious radiation heat loss and the effect of heat radiation is less at higher temperatures. Although higher temperature of GF would lead to larger heat loss to the environment, the radiation inside GF at high temperature could contribute more to thermal conductivity of GF. Therefore, it could be possible that at high Joule heating power, the ratio of radiation heat loss to the environment could decrease due to larger thermal conductance effect. In fact the effect of radiation heat transfer on thermal conductivity measurement is smaller than the effect caused by samples difference and can be totally neglected. The exclusion of radiation effect on the thermal diffusivity fitting is studied by Lin *et al* [16] and their theoretic analysis gave the following solution as $T^* = 96/\pi^4\sum_{m=1}^{\infty}\left\{1 - \exp\left[-(2m-1)^2\pi^2\alpha_{\mathrm{eff}}t/L^2\right]\right\}/(2m-1)^4$, almost the same with the solution without considering radiation except that α is replaced by α_{eff}. The expression for α_{eff} is $\alpha_{\mathrm{eff}} = \alpha + 8\varepsilon_r\sigma T_0^3 L^2/\rho c_p D\pi^2$, where D is the thickness of GF. We can estimate the value of radiation part as 4.25×10^{-6} m^2 s^{-1} by assuming the mass density of 10 kg m^{-3}, length of 5 mm, thickness of 1 mm, which is more

than one magnitude smaller than our measured values. In our experiment, an aluminum foil is used to fold the sample stage to eliminate the radiation effect. Therefore, the effect of radiation heat loss can be ignored.

4. Conclusion

In summary, a strong temperature dependence of thermal properties of GF is revealed in this work. Thermal conductivity and thermal diffusivity of GF are improved significantly from ~0.3 to 1.5 $W\,m^{-1}\,K^{-1}$ and from $\sim 4\times10^{-5}$ to $\sim 2\times10^{-4}\,m^2\,s^{-1}$ respectively with respect to temperature from 310 K to 440 K, which is an abnormal phenomenon cannot be explained through Umklapp scattering theory for single crystal structures of carbon materials. The measured low thermal conductivity is attributed to the high porosity and numerous thermal contacts inside sample. Our quantitative analysis shows the thermal contact resistance of graphene flakes is much larger than intrinsic thermal resistance inside graphene for temperature below 450 K. The improved thermal property of GF at higher temperatures can be explained through the reduction in thermal contact resistance due to the tighter contact induced by thermal expansion effect and partly the improved radiation heat exchange inside the pore of GF. The finding of temperature dependence of thermal transport of GF is beneficial for thermal design of GF based thermal energy applications such as Li-ion batteries working in such temperature range.

Acknowledgments

Authors gratefully thank the financial support from National Natural Science Foundation of China (Nos. 51206124 and 51428603) and SRF for ROCS, SEM.

References

[1] Geim A K 2009 Graphene: status and prospects *Science* **324** 1530–4
[2] Chen Z, Ren W, Gao L, Liu B, Pei S and Cheng H-M 2011 Three-dimensional flexible and conductive interconnected graphene networks grown by chemical vapour deposition *Nat. Mater.* **10** 424–8
[3] Cao X, Shi Y, Shi W, Lu G, Huang X, Yan Q, Zhang Q and Zhang H 2011 Preparation of novel 3D graphene networks for supercapacitor applications *Small* **7** 3163–8
[4] Dong X, Cao Y, Wang J, Chan-Park M B, Wang L, Huang W and Chen P 2012 Hybrid structure of zinc oxide nanorods and three dimensional graphene foam for supercapacitor and electrochemical sensor applications *R. Soc. Chem. Adv.* **2** 4364–9
[5] Wang W, Guo S, Penchev M, Ruiz I, Bozhilov K N, Yan D, Ozkan M and Ozkan C S 2013 Three dimensional few layer graphene and carbon nanotube foam architectures for high fidelity supercapacitors *Nano Energy* **2** 294–303
[6] Zhao Y, Liu J, Hu Y, Cheng H, Hu C, Jiang C, Jiang L, Cao A and Qu L 2013 Highly compression-tolerant supercapacitor based on polypyrrole-mediated graphene foam electrodes *Adv. Mater.* **25** 591–5
[7] Chen Z, Xu C, Ma C, Ren W and Cheng H-M 2013 Lightweight and flexible graphene foam composites for high-performance electromagnetic interference shielding *Adv. Mater.* **25** 1296–300
[8] Ji H, Zhang L, Pettes M T, Li H, Chen S, Shi L, Piner R and Ruoff R S 2012 Ultrathin graphite foam: a three-dimensional conductive network for battery electrodes *Nano Lett.* **12** 2446–51
[9] Li N, Chen Z, Ren W, Li F and Cheng H-M 2012 Flexible graphene-based lithium ion batteries with ultrafast charge and discharge rates *Proc. Natl Acad. Sci. USA* **109** 17360–5
[10] Balandin A A, Ghosh S, Bao W, Calizo I, Teweldebrhan D, Miao F and Lau C N 2008 Superior thermal conductivity of single-layer graphene *Nano Lett.* **8** 902–7
[11] Nika D L, Pokatilov E P, Askerov A S and Balandin A A 2009 Phonon thermal conduction in graphene: role of Umklapp and edge roughness scattering *Phys. Rev.* B **79** 155413
[12] Koh Y K, Bae M-H, Cahill D G and Pop E 2010 Heat conduction across monolayer and few-layer graphenes *Nano Lett.* **10** 4363–8
[13] Seol J H *et al* 2010 Two-dimensional phonon transport in supported graphene *Science* **328** 213–6
[14] Pop E, Varshney V and Roy A K 2013 Thermal properties of graphene: fundamentals and applications *MRS Bull.* **37** 1273–81
[15] Pettes M T, Ji H, Ruoff R S and Shi L 2012 Thermal transport in three-dimensional foam architectures of few-layer graphene and ultrathin graphite *Nano Lett.* **12** 2959–64
[16] Huan L, Shen X, Xinwei W and Ning M 2013 Significantly reduced thermal diffusivity of free-standing two-layer graphene in graphene foam *Nanotechnology* **24** 415706
[17] Konatham D, Papavassiliou D and Striolo A 2012 Thermal boundary resistance at the graphene–graphene interface estimated by molecular dynamics simulations *Chem. Phys. Lett.* **527** 47–50
[18] Yue Y, Zhang J and Wang X 2011 Micro/nanoscale spatial resolution temperature probing for the interfacial thermal characterization of epitaxial graphene on 4 H–SiC *Small* **7** 3324–33
[19] Zhang X, Yeung K K, Gao Z, Li J, Sun H, Xu H, Zhang K, Zhang M, Chen Z and Yuen M M 2014 Exceptional thermal interface properties of a three-dimensional graphene foam *Carbon* **66** 201–9
[20] Pop E, Mann D, Wang Q, Goodson K and Dai H 2005 Thermal conductance of an individual single-wall carbon nanotube above room temperature *Nano Lett.* **6** 96–100
[21] Yue Y, Liu K, Li M and Hu X 2014 Thermal manipulation of carbon nanotube fiber by mechanical stretching *Carbon* **77** 973–9
[22] Aliev A E, Guthy C, Zhang M, Fang S, Zakhidov A A, Fischer J E and Baughman R H 2007 Thermal transport in MWCNT sheets and yarns *Carbon* **45** 2880–8
[23] Guo J, Wang X and Wang T 2007 Thermal characterization of microscale conductive and nonconductive wires using transient electrothermal technique *J. Appl. Phys.* **101** 063537
[24] Jang W, Chen Z, Bao W, Lau C N and Dames C 2010 Thickness-dependent thermal conductivity of encased graphene and ultrathin graphite *Nano Lett.* **10** 3909–13
[25] Balandin A A 2011 Thermal properties of graphene and nanostructured carbon materials *Nat. Mater.* **10** 569–81
[26] Gonnet P, Liang Z, Choi E S, Kadambala R S, Zhang C, Brooks J S, Wang B and Kramer L 2006 Thermal conductivity of magnetically aligned carbon nanotube buckypapers and nanocomposites *Curr. Appl. Phys.* **6** 119–22

[27] Schuetz M and Glicksman L 1984 A basic study of heat transfer through foam insulation *J. Cell. Plast.* **20** 114–21
[28] Incropera F P 2011 *Fundamentals of Heat and Mass Transfer* (New York: Wiley)
[29] Chen S *et al* 2010 Raman measurements of thermal transport in suspended monolayer graphene of variable sizes in vacuum and gaseous environments *ACS Nano* **5** 321–8
[30] Chen S, Wu Q, Mishra C, Kang J, Zhang H, Cho K, Cai W, Balandin A A and Ruoff R S 2012 Thermal conductivity of isotopically modified graphene *Nat. Mater.* **11** 203–7
[31] Nelson J B and Riley D P 1945 The thermal expansion of graphite from 15 °C to 800 °C: I. Experimental *Proc. Phys. Soc.* **57** 477
[32] Jiang J-W, Wang J-S and Li B 2009 Thermal expansion in single-walled carbon nanotubes and graphene: nonequilibrium green's function approach *Phys. Rev.* B **80** 205429
[33] Bao W, Miao F, Chen Z, Zhang H, Jang W, Dames C and Lau C N 2009 Controlled ripple texturing of suspended graphene and ultrathin graphite membranes *Nat. Nano* **4** 562–6
[34] Tsang D K L, Marsden B J, Fok S L and Hall G 2005 Graphite thermal expansion relationship for different temperature ranges *Carbon* **43** 2902–6
[35] Prasher R S, Hu X J, Chalopin Y, Mingo N, Lofgreen K, Volz S, Cleri F and Keblinski P 2009 Turning carbon nanotubes from exceptional heat conductors into insulators *Phys. Rev. Lett.* **102** 105901